J Mater Sci (2008) 43:3775–3781
DOI 10.1007/s10853-007-2394-z

Coercivity and domain structure of nanograined Fe–C alloys after high-pressure torsion

Svetlana G. Protasova · Boris B. Straumal · Sergei V. Dobatkin · Dagmar Goll · Gisela Schütz · Brigitte Baretzky · Andrei A. Mazilkin · Alexei N. Nekrasov

Received: 6 July 2007 / Accepted: 7 December 2007 / Published online: 6 March 2008

Abstract The microstructure and magnetic properties of binary hypo- and hyper-eutectoid Fe–C alloys were studied. The investigations have been carried out on the samples in the as-cast state, after a long annealing at 725 °C and on the specimens after the high-pressure torsion (HPT). The deformation was carried out at the ambient temperature and the pressure of 5 GPa. The grain size after HPT is in the nanometer range. Long annealing leads to a drastic decrease of the coercivity in comparison with the as-cast alloys. In all alloys the coercivity H_c increases with increasing carbon content. The distance L between pinning points for domain walls decreases with increasing carbon content. Increase of the coercivity and decrease of L are more pronounced below the eutectoid concentration. The coercivity of the nanostructured samples is higher than that of the as-cast alloys. Due to the pinning of domain walls by the cementite particles, the hysteresis loop in the coarse-grained alloys both in as-cast and annealed states has a narrowing near the zero magnetization.

S. G. Protasova (✉) · B. B. Straumal · A. A. Mazilkin
Institute of Solid State Physics, Russian Academy of Sciences, Chernogolovka, Moscow 142432, Russia
e-mail: sveta@issp.ac.ru

B. B. Straumal · D. Goll · G. Schütz · B. Baretzky
Max-Planck-Institut für Metallforschung, Heisenbergstrasse 3, 70569 Stuttgart, Germany

S. V. Dobatkin
A.A. Baikov Institute of Metallurgy and Materials Science, Russian Academy of Sciences, Leninsky prosp. 49, 119991 Moscow, Russia

A. N. Nekrasov
Institute of Experimental Mineralogy, Russian Academy of Sciences, Chernogolovka, Moscow district 142432, Russia

Introduction

The study of nanocrystalline solids increased pronouncedly in the last decade. The interest is driven by the unique physical and mechanical properties of these materials. Among the most important techniques for nanograined polycrystal preparation, one can mention gas condensation, ball milling, crystallization from amorphous state, and severe plastic deformation (SPD) techniques. SPD techniques, such as high pressure torsion (HPT), do not cause changes in the material geometry, in the contrast to the conventional processes of high deformation like rolling or wire drawing [1–3]. The properties of newly developed nanostructured materials are defined in turn by their structural features. Therefore, the comprehensive investigation of nanograined polycrystals in the alloying systems, which are most important for the structural and functional applications, is crucial. The aim of this work is to study the influence of the microstructure on domain structure and coercivity in coarse-grained and nanograined Fe–C alloys within a broad interval of carbon concentrations.

Experimental

Both hypo- and hyper-eutectoid Fe–C alloys with carbon concentration of 0.25, 0.45, 0.60, 1.3, 1.5, and 1.7 wt.% were prepared from high-purity 5 N iron and graphite by a vacuum induction melting in a form of cylindrical ingots. For HPT treatment the 0.4 mm thick discs were cut from the as-cast

ingots, then ground and chemically etched. They were subjected to HPT at room temperature (5 torsions under a pressure of 5 GPa in a Bridgman anvil-type unit, shear strain was about 6). Samples for structural and magnetic investigations were cut from the HPT-deformed discs at a distance of 3 mm from the sample center. A set of the as-cast samples with 0.25, 0.60, 1.3, and 1.7 wt.% was additionally annealed during 950 h at 725 °C (i.e., below the eutectoid temperature) in order to achieve the equilibrium $\alpha + Fe_3C$ structure. Light microscopy (LM) was performed on a Zeiss Axiophot microscope. For the metallographic investigations the samples were ground by SiC grinding paper, polished with 6, 3, and 1 μm diamond pastes and etched for 5–10 s with a 5 wt.% HNO_3 solution in ethyl alcohol. Magnetic measurements were performed using a vibrating sample magnetometer (VSM). Magnetic field in the VSM was applied parallel to the sample plane. Transmission electron microscopy (TEM) investigations were carried out on a JEM–4000FX microscope with an accelerating voltage of 400 kV. Domain structure of the samples was visualized on a magnetic force microscopic facility.

Results and discussion

Structural investigations

Samples after HPT

Figure 1 shows bright (Fig. 1a) and dark (Fig. 1b) field TEM micrographs of the Fe –0.25 wt.% C alloy. The electron diffraction pattern (Fig. 1a, insert) contains only α-Fe and Fe_3C spots. The TEM micrographs and electron diffraction patterns of Fe alloys with 0.45, 0.60, 1.3, 1.5, and 1.7 wt.% C after HPT are very similar to those shown in Fig. 1. Both the ferrite grains and cementite particles are visible in the dark field image (Fig. 1b) as the reflections of these phases lie closely to each other. Ferrite grain size after HPT is about 100 nm. However, there are some ferrite grains with the size about 400 nm. Grain size increases with increasing carbon content. Ferrite grains are not equiaxial, they are slightly elongated parallel to the deformation direction. Cementite grain size in all studied alloys is about 10 nm. They are more or less uniformly distributed over the specimen and more equiaxial than elongated ferrite grains. The spacing between the cementite particles decreases with increasing carbon content. It is about 50–100 nm in Fe–0.25 wt.% C alloy and about 10–50 nm in the Fe–1.7 wt.% C alloy. Only two phases, namely α-Fe and Fe_3C are present after HPT in all studied alloys. No signs of retained austenite, graphite, or other iron carbides are present in the electron diffraction patterns.

Coarse-grained as-cast alloys

In Fig. 2, the microstructures of the as-cast alloys obtained by LM are shown. The structure depends on the carbon content. In the alloy with 0.25 wt.% C (Fig. 2a) the following structural components are present: (a) the austenite grains transformed into ferrite + austenite mixture during the cooling through the ferrite + austenite region of the Fe–C phase diagram; (b) the initial austenite plates transformed into perlite or troostite and appear grey; (c) the ferrite layers along the grain boundaries (GBs) of the transformed austenite (primary ferrite) appear white. The Widmanstätten plates, growing from the GB ferrite, are visible. Figure 2b shows that at 0.45 wt.% C the amount of the primary ferrite decreases with increasing carbon content. The microstructure of hyperetectoid steels with 1.5 (Fig. 2c) and 1.7 wt.%C (Fig. 2d) differs from that of hypoetectoid alloys (Fig. 2a and b). It contains the initial austenite grains transformed into troostite which appears gray. GBs between former austenite grains are covered by the cementite layers. The Widmanstätten plates growing from the GB cementite are visible. The amount of the primary cementite (and also the number of cementite Widmanstätten plates) increases with increasing carbon content. Electron and X-ray diffraction show the presence of the retained austenite and do not show any presence of graphite in all studied samples.

Samples annealed at 725 °C and quenched in cold water

In Fig. 3, the LM microstructure of the Fe–C alloys with 0.25, 0.6, 1.3, and 1.7 wt.% of carbon, annealed during 950 h at 725 °C to achieve the equilibrium $\alpha + Fe_3C$ structure, are shown. After long annealing the structure of hypoeutectoid and hypereutectoid alloys became very similar. All the samples contain very coarse ferrite and cementite grains. Only the amount of cementite is different; it increases with increasing carbon content according to the Fe–C phase diagram.

Magnetic measurements

Coercivity

The dependence of $\mu_0 H_c$ (μ_0 is the permeability of free space) on carbon concentration is presented in Fig. 4. The coercivity of the nanostructured samples after HPT is higher than that of the coarse-grained as-cast and annealed alloys.

The resulted plot for the as-cast alloys is obviously composed of two parts: the first line with a large slope is for hypoeutectoid alloys and another almost horizontal one

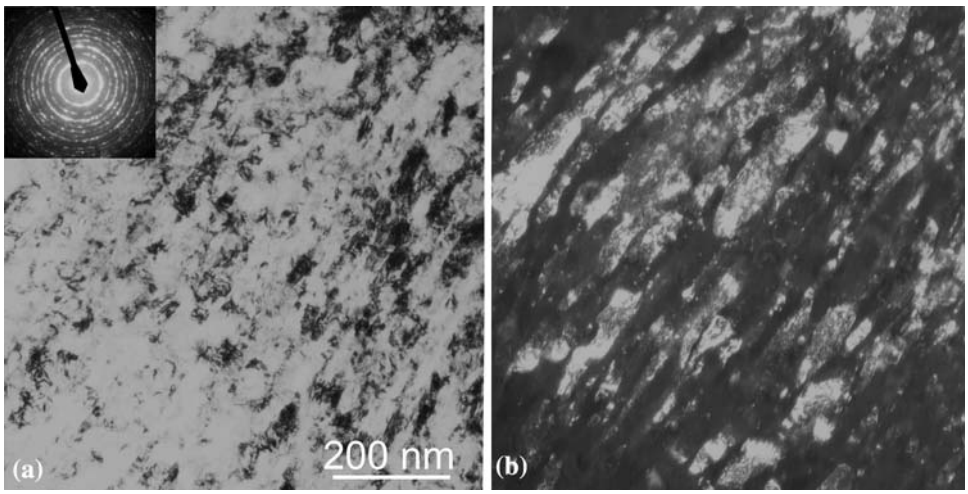

Fig. 1 Bright (**a**) and dark (**b**) field TEM micrographs of the Fe–0.25 wt.% C alloy after HTP. Electron diffraction pattern revealing α-Fe and Fe_3C spots is shown in the insert

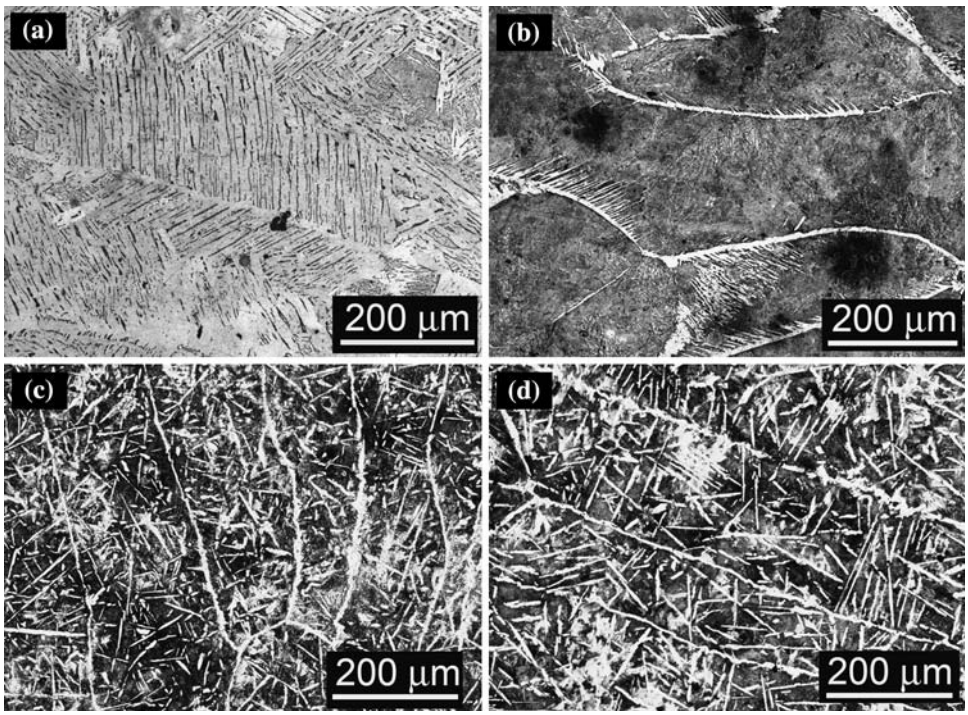

Fig. 2 Light micrographs of as-cast Fe–C alloys with 0.25 (**a**), 0.45 (**b**), 1.5 (**c**) and 1.7 (**d**) wt.% C. The austenite is transformed into troostite and appears grey in all micrographs. In (**a**) and (**b**) ferrite appears white. In (**c**) and (**d**) cementite appears white

corresponds to the hypereutectoid alloys. Such a behavior can be understood if we compare the microstructure of the low carbon and high carbon alloys. At the low carbon concentrations, the amount of α-Fe is high (Fig. 2a), and the magnetization vector can easily change its direction with changing the external magnetic field. With increasing carbon content the amount of cementite increases and the distance between Fe_3C platelets or particles decreases (Fig. 2b). At 0.6 wt.% C the easily magnetized primary ferrite grains almost disappear from the microstructure. The austenite grains are transformed into the fine-lamellar troostite.

In the microstructure of all studied alloys after HPT, no significant changes with the change of carbon concentration are observed. The cementite nanoparticles are finely dispersed among the nanometric ferrite grains. After long annealing below the eutectoid temperature, the differences between hypo- and hyper-eutectoid as-cast alloys also disappear (Figs. 3, 4).

The dependence of the coercivity on carbon concentration (Fig. 4) can be discussed based on the Kersten model [10–12]. In this model, it is assumed that the domain walls move by the magnetization through the array of pinning points. If the external magnetic field increases, the pinned domain wall bends first and jumps to the next couple of the pining points after that. Pores, dislocations, or particles of a second phase may act as pinning points. Coercivity H_c in this case is defined by the equation

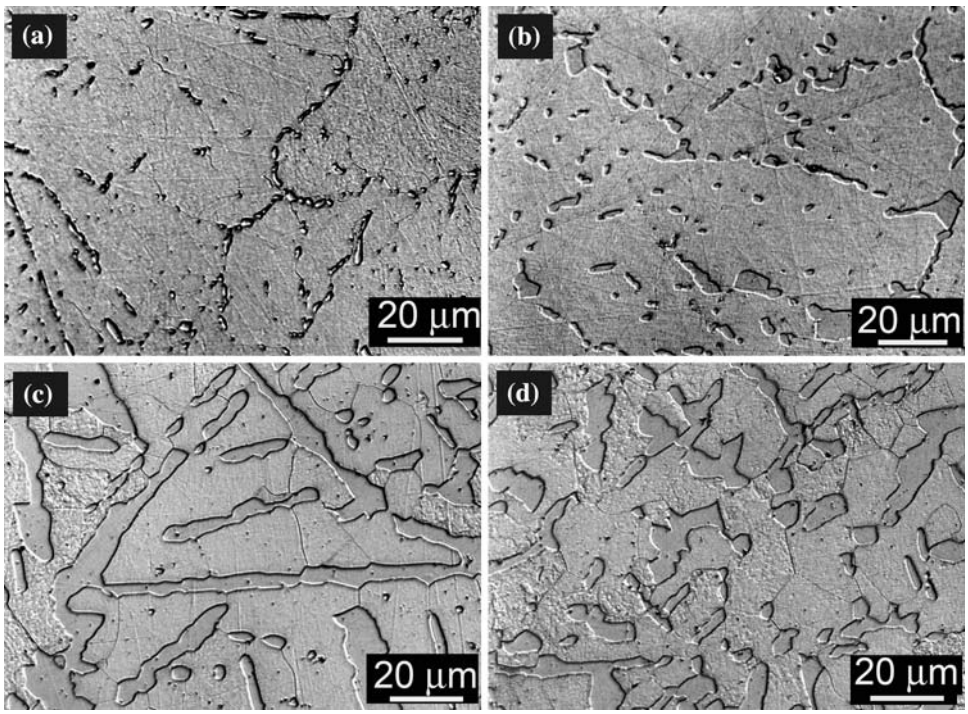

Fig. 3 Light micrographs of the Fe–C alloys with 0.25 wt.% C (**a**), 0.6 wt.% C (**b**), 1.3 wt.% C (**c**) and 1.7 wt.% C (**d**) annealed at 725 °C, 950 h (below the eutectoid temperature)

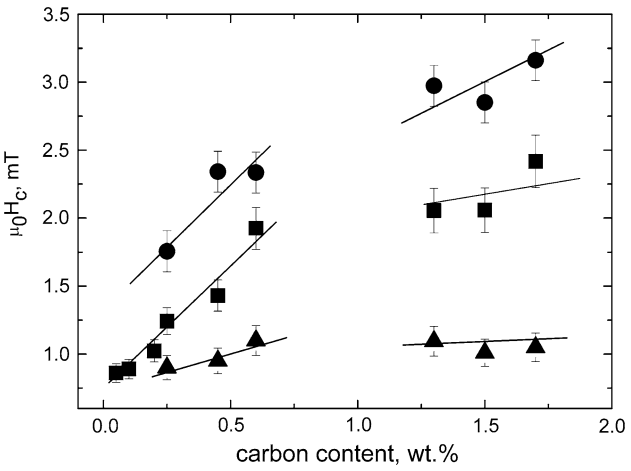

Fig. 4 Dependence of $\mu_0 H_c$ on carbon concentration for as-cast alloys (■), samples after HPT (●) and after annealing at 725 °C, 950 h (▲). Straight lines are guides for the eye

$$H_c = \gamma/(J_s L \cos\theta), \quad (1)$$

where γ is the surface energy of a domain wall (the value for pure Fe is used $\gamma = 1.6{\cdot}10^{-3}$ J/m^2 [13] since the data for carbon-containing ferrite are not available in the literature), J_s is the saturation magnetization, θ is the angle between external magnet field vector and magnetization vector, and L is the mean distance between pinning points. It should be noted that this model is used as the simplest existing one in order to make the estimations of L. In case when several mechanisms of the magnetization reversal are involved it seems not to describe the process well. Nevertheless, the calculations gave the L values roughly equal to the distance between the cementite particles for all three states of the alloys.

Using the data obtained in [9] and supposing $\cos\theta = 1$, we have estimated the distance between pinning points for the alloys with various carbon concentrations (Fig. 5). Two linear dependencies can be plotted for the as-cast alloys: the first one with a large slope for the hypoeutectoid alloys and the second almost horizontal for hypereutectoid alloys. Like in the preceding discussion of the coercivity behavior, the L vs. carbon content dependence can be explained from

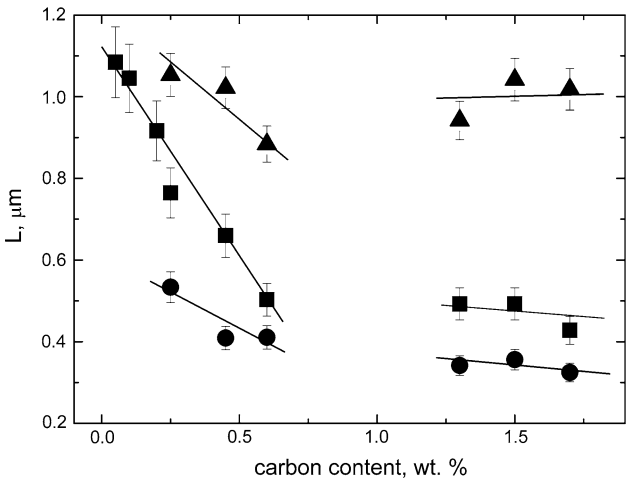

Fig. 5 Distance L between pinning points calculated based on the Kersten model [10–12] for various carbon concentrations: as-cast alloys (■); after HPT (●); annealed at 725 °C, 950 h (▲)

the structural features of the studied alloys. At low carbon concentration and high amount of α-Fe the value of L (about 1–2 μm) can be identified with the distance between minor cementite platelets or particles. The distance between Fe_3C platelets or particles decreases with increasing carbon content (see Fig. 2). The mean interlamellar distance in the troostite for 0.6 wt.% carbon corresponds well to the distance between pinning points obtained from the Eq. 1. In all alloys with carbon concentration above 0.6 wt.% lamellar troostite remains the main component in the structure (Fig. 2c and d). The TEM results reveal that the interlamellar distance in the troostite does not change much between 0.6 and 1.7 wt.% C. The distance between pinning points calculated using the Eq. 1 also slowly decreases in this concentration interval.

L is lower for all HPT alloys comparing with as-cast alloys. After HPT the microstructure of all studied alloys does not change much with carbon concentration. In other words, there is no such a drastic difference between the hypo- and hyper-eutectoid as-cast alloys. TEM revealed that the mean distance between the cementite particles slowly decreases with increasing carbon content. Long annealing below the eutectoid temperature also resulted in disappearance of structural differences for the alloys with different carbon concentrations (Fig. 5). L strongly decreases with increasing carbon concentration below the eutectoid concentration (0.8 wt.% C) and slowly decreases above it. The decrease of L value is especially pronounced for the as-cast alloys, because the distances between ferrite and cementite plates decrease with increasing carbon concentration stronger than for the samples after HPT and long annealing (Figs. 1–3). Therefore, the pinning of the magnetic domain walls is governed by the size and the arrangement of the cementite grains. These facts are perfectly reflected in the behavior of mean distance between the pinning points for the annealed alloys and alloys after HPT.

Domain structure

It has been observed that hysteresis loops for the HPT samples differ from those for the coarse-grained (as-cast and annealed) alloys (Fig. 6). In the latter case, the hysteresis loops are narrower around the zero magnetization and broader near the saturation magnetization (Fig. 6a). To the opposite, the hysteresis loops of the samples after HPT do not demonstrate such a shrinkage-broadening behavior (Fig. 6b).

We assume that this difference may arise from the alterations in magnetization mechanism of the samples, which are determined in turn by the microstructure. In Fig. 7 the images of domain structure for the samples without applied magnetic field are shown. Distinct correlation of the microstructure and domain structure both for the as-cast coarse-grained samples and samples after HPT is visible. The size of magnetic domains in the as-cast samples decreases with increasing carbon concentration (compare Fig. 7a and b) similar to the grain size. After HPT the magnetic domains are much smaller

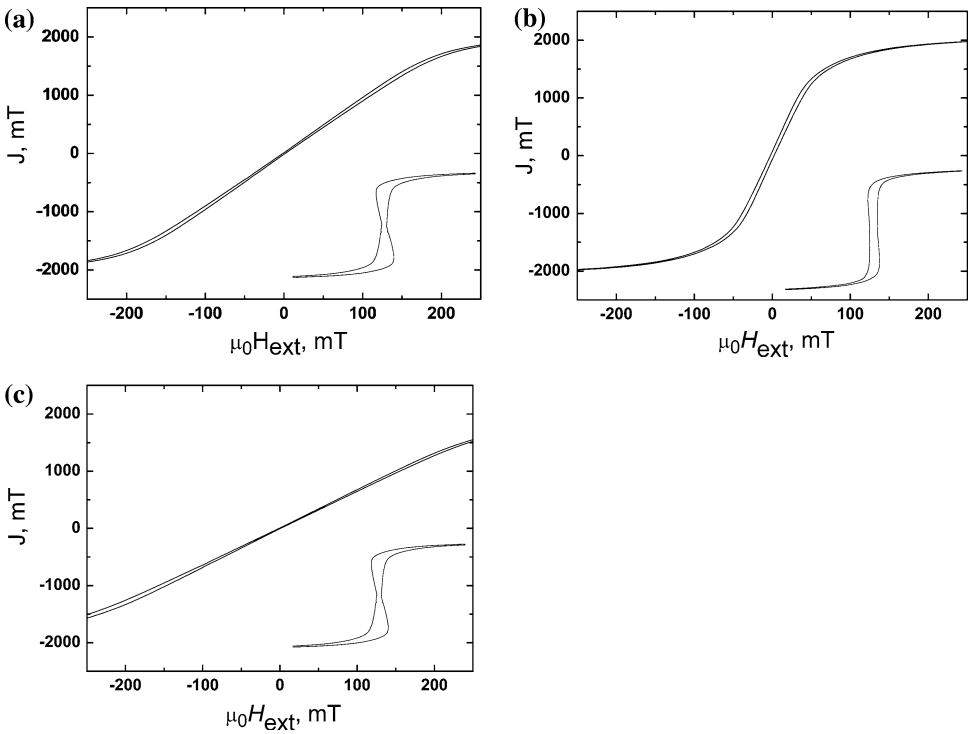

Fig. 6 Central part of the experimental hysteresis loops for the samples with 0.45 wt.% C (**a**) as-cast (**b**) after HPT and (**c**) annealed at 725 °C, 950 h. Schematic drawings of the hysteresis loops shape are presented in the inserts

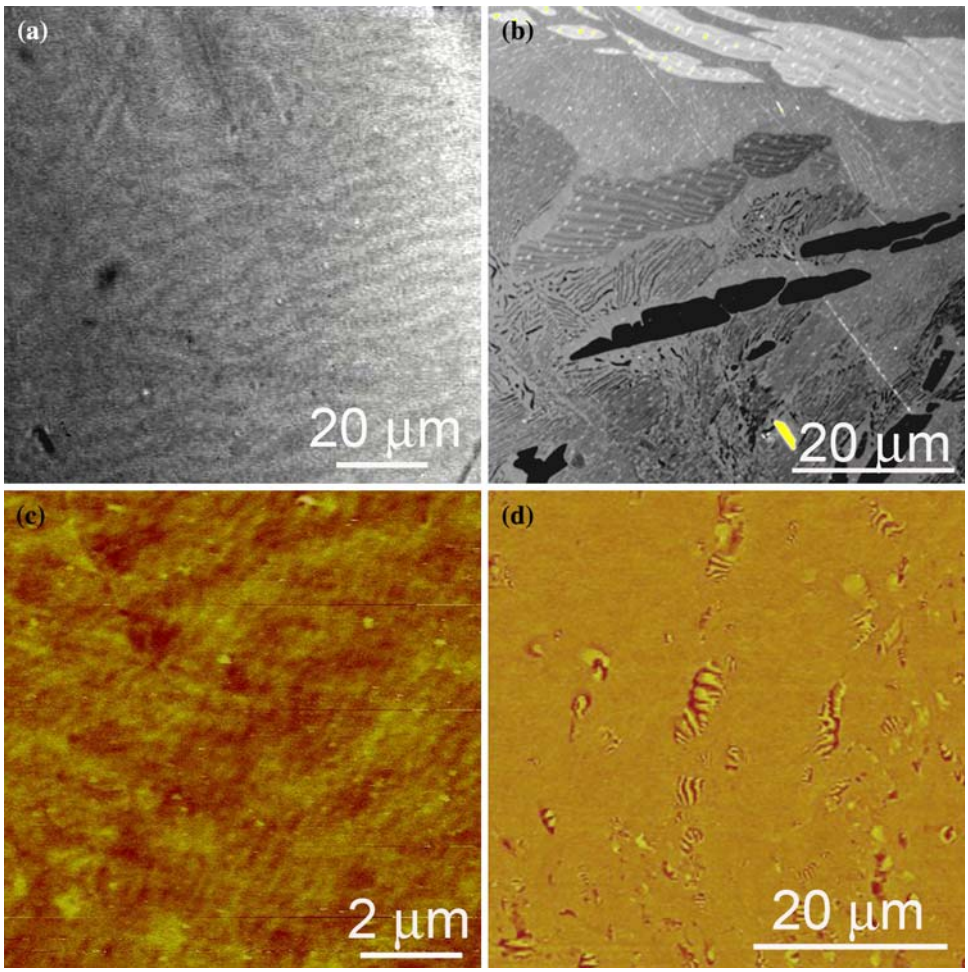

Fig. 7 Domain structure for the coarse-grained as-cast alloys with 0.25 wt.% C (**a**) and 1.7 wt.%C (**b**), and samples after HPT with 0.25 wt.%C (**c**) and 1.7 wt.%C (**d**)

than in the as-cast alloys. Domains in the samples after HPT are equiaxial in shape in contrast to the elongated domains in the as-cast alloys (compare Fig. 7c and d). The microstructure of the samples after HPT looks like a uniform mixture of ferrite and cementite grains (Fig. 1). In the Fe–1.7 wt.% C alloy this mixture surrounds also few large ferrite grains. Fine cementite particles cannot strongly influence the movement of domain walls in the magnetic field. To the opposite, the cementite particles in the as-cast samples are large and can serve as obstacles for the domain wall movement. By increasing external magnetic field further magnetization proceeds due to the rotation of magnetic moment in each domain. Therefore, the domain structure becomes pseudo-single-domain. This is the reason for the shrinkage of the hysteresis loops around the zero magnetization.

Conclusions

High-pressure torsion of the studied Fe–C alloys leads to the grain size refinement down to the nanometer range and increase of the coercivity. Long annealing leads to the drastic decrease of the coercivity in comparison with the as-cast alloys. In all alloys the coercivity H_c and the distance L between pinning points for domain walls decreases with increasing carbon content. Increase of H_c and decrease of L is more pronounced below the eutectoid concentration. Due to the pinning of the domain walls by the cementite particles, the hysteresis loop in the coarse-grained (as-cast and long-annealed) alloys has a narrowing near the zero magnetization.

Acknowledgements The authors thank the Russian Foundation for Basic Research (contracts 06-03-32875 and 05-02-16528) and the INTELS foundation for science and education (contract G-35-06-01). They also greatly appreciate Mrs. T. Dragon's (Max-Planck-Institut für Metallforschung, Stuttgart) help with the sample preparation for the domain structure investigations.

References

1. Shabashov VA, Korshunov LG, Mukoseev AG, Sagaradze VV, Makarov AV, Pilyugin VP, Novikov SI, Vildanova NF (2003) Mater Sci Eng A 346A:196
2. Ivanisenko Yu, Lojkovski W, Valiev RZ, Fecht H-J (2003) Acta Mater 51:5555

3. Ivanisenko Yu, MacLaren I, Valiev RZ, Fecht H-J (2005) Adv Eng Mater 7:1011
4. Ivanisenko Yu, MacLaren I, Sauvage X, Valiev RZ, Fecht H-J (2006) Acta Mater 54:1659
5. Amilis X, Nogués J, Suriñach S, Muriños JS, Baró MD (2001) Phys Rev B 63B:052402
6. Del Bianco L, Hernando A (1997) Phys Rev B 56B:8894
7. Li M, Birringer R, Johnson WL (1993) Nanostruct Mater 3:407
8. Read HG, Reynolds Jr. WT, Hono K, Tarui T (1997) Scripta Mater 37:1221
9. Straumal BB, Mazilkin AA, Protasova SG, Dobatkin SV, Rodin AO, Baretzky B, Goll D, Schütz G (2007) Acta Mater (to be published)
10. Kersten M (1956) Zt angew Phys 7:313
11. Kersten M (1956) Zt angew Phys 8:382
12. Kersten M (1956) Zt angew Phys 8:496
13. Chikazumi S (1964) Physics of magnetism. Wiley, NY